Influence of magnetic shear on impurity transport

H. Nordman and T. Fülöp
Department of Radio and Space Science, Chalmers University of Technology and Euratom-VR Association, Göteborg, Sweden

J. Candy
General Atomics, P.O. Box 85608, San Diego, California 92186-5608

P. Strand and J. Weiland
Department of Radio and Space Science, Chalmers University of Technology and Euratom-VR Association, Göteborg, Sweden

(Received 19 December 2006; accepted 22 March 2007; published online 4 May 2007)

The magnetic shear dependence of impurity transport in tokamaks is studied using a quasilinear fluid model for ion temperature gradient (ITG) and trapped electron (TE) mode driven turbulence in the collisionless limit and the results are compared with nonlinear gyrokinetic results using GYRO [J. Candy and R. E. Waltz, J. Comput. Phys **186**, 545 (2003)]. It is shown that the impurity transport is sensitive to the magnetic shear, in particular for weak, negative, and large positive shear where a strong reduction of the effective impurity diffusivity is obtained. The fluid and gyrokinetic results are in qualitative agreement, with the gyrokinetic diffusivities typically a factor 2 larger than the fluid diffusivities. The steady state impurity profiles in source-free plasmas are found to be considerably less peaked than the electron density profiles for moderate shear. Comparisons between anomalous and neoclassical transport predictions are performed for ITER-like profiles [R. Aymar, P. Barabaschi, and Y. Shimomura, Plasma Phys. Controlled Fusion **44**, 519 (2002)]. © *2007 American Institute of Physics*. [DOI: 10.1063/1.2730491]

I. INTRODUCTION

Improving the understanding of impurity transport in tokamaks is one of the major tasks in present fusion research. Impurities can, if transported to the plasma core, cause fuel dilution, severe radiated power loss and an uncontrolled impurity accumulation may even terminate the discharge. There are several experimental indications that impurity transport may depend on the magnetic shear. In the Joint European Torus (JET) (Ref. 1) and Tore Supra (Ref. 2) low-confinement mode discharges, it has been shown that there are two impurity transport regions: the central core having low impurity transport coefficients and an outer region with larger impurity transport coefficients.[3,4] The position of the transition layer between low and high impurity transport coefficients has been connected to the $s=0.5$ flux surface, where $s=(r/q)dq/dr$ and q is the safety factor. No dependence on the impurity charge number has been observed. In ASDEX,[5] the impurity diffusion coefficient was found to be low in the center and rise exponentially with the radial distance from the center, in a way that can be interpreted as a quite steep transition at a certain value of the shear.[6] In a systematic comparison of hybrid scenario discharges (i.e., discharges with a weak magnetic shear over a large part of the plasma cross section) with standard ELMy H-mode discharges[7] a somewhat more peaked electron and impurity density profile has been observed, although this may be a result of the lack of sawteeth in hybrid scenarios rather than a result of shear dependence of transport.

Models of impurity transport driven by ITG/TE mode turbulence[8–13] and neoclassical effects[14] are now well developed. Comparisons of anomalous and neoclassical transport for JET discharges[15] and ITER-like plasmas have also been performed.[16] However, the magnetic shear dependence of impurity transport has not been investigated theoretically in any detail. In the present study a quasilinear fluid model[10,17] for ITG/TE mode driven turbulence is used in the collisionless limit to elucidate the magnetic shear dependence of anomalous impurity transport. The fluid results obtained using an analytical approach valid for general mode width[18] are compared with the fluid results of a strong ballooning analysis[19] and with nonlinear gyrokinetic simulation results. In addition, comparisons of anomalous and neoclassical predictions of impurity flux are performed for ITER-like profiles.

The structure of the paper is the following: In Sec. II the models used to determine the turbulent and neoclassical impurity transport in the collisionless regime are described. Section III discusses the magnetic shear dependence of the impurity transport. In Sec. IV turbulent and neoclassical impurity particle fluxes are compared for a hybrid ITER scenario.[20] Finally, the results are summarized in Sec. V.

II. IMPURITY TRANSPORT

We assume that the total impurity transport is a linear sum of turbulence-driven transport and neoclassical transport. This assumption has been confirmed experimentally[21] and it is justified by the fact that neoclassical transport is driven by parallel friction dynamics, and is not affected significantly by the ion cross-field transport which is dominated by fluctuations.

A. Turbulent transport

A set of fluid equations is used for the perturbations in density, parallel velocity, and pressure,[10,11,17,23]

$$\frac{\partial n_j}{\partial t} + \nabla \cdot (n_j \boldsymbol{v}_j) = 0, \tag{1}$$

$$m_{i,z} n_{i,z} \frac{\partial v_{\|i,z}}{\partial t} + \nabla_\| (n_{i,z} T_{i,z}) + n_{i,z} e \nabla_\| \phi = 0, \tag{2}$$

$$\frac{3}{2} n_j \frac{dT_j}{dt} + n_j T_j \nabla \cdot \boldsymbol{v}_j + \nabla \cdot \boldsymbol{q}_j = 0, \tag{3}$$

where $j=i$, z, et represent ions, impurities, and trapped electrons, n_j, $v_{\|i,z}$, T_j, are the density, parallel velocity, and temperature perturbations, ϕ is the perturbed electrostatic potential, $\boldsymbol{v}_j = \boldsymbol{v}_E + \boldsymbol{v}_{*j} + \boldsymbol{v}_{pj} + \boldsymbol{v}_{\pi j}$, $\boldsymbol{v}_E$ is the $\boldsymbol{E}\times\boldsymbol{B}$ velocity, $\boldsymbol{v}_{*j}$ is the diamagnetic drift velocity,

$$\boldsymbol{v}_{pj} = \frac{d\boldsymbol{E}}{dt} \Big/ (B\Omega_{cj}) \tag{4}$$

is the polarization drift velocity,

$$\boldsymbol{v}_{\pi j} = \frac{\boldsymbol{e}_\| \times \nabla \cdot \pi_j}{Z_j e n_j B} \tag{5}$$

is the drift due to the off-diagonal elements of the stress tensor, and

$$\boldsymbol{q}_j = \frac{5}{2} \frac{p_j}{m_j \Omega_{cj}} (\boldsymbol{e}_\| \times \nabla T_j) \tag{6}$$

is the diamagnetic heat flux, where Ω_{cj} is the cyclotron frequency. The derivative is defined as $d/dt = \partial/\partial t + \boldsymbol{v}_E \cdot \nabla$. The electrostatic limit is considered, where the free electron density perturbation is related to the perturbed electric potential ϕ by the adiabatic condition $\delta n_{ef}/n_{ef} = e\phi/T_e$. Assuming quasineutrality, we have $\delta n_e/n_e = \delta n_{et}/n_e + \delta n_{ef}/n_e = (1 - Zf_z)\delta n_i/n_i + Zf_z \delta n_z/n_z$, where $f_z = n_z/n_e$ is the impurity fraction, and δn_z is the impurity density perturbation due to the turbulence given by[10]

$$\frac{\delta n_z}{n_z} = \frac{L_{ne}}{L_{nz}} \frac{\omega_{\star e}}{N_z} \left[\omega(1 - \epsilon_{nz}) + \left(\eta_z - \frac{7}{3} + \frac{5}{3}\epsilon_{nz} \right) \omega_{Dz} \right] \frac{e\phi}{T_e} \tag{7}$$

where $N_z = \omega^2 - 10\omega\omega_{Dz}/3 + 5\omega_{Dz}^2/3$, $\omega_{\star j}$ is the diamagnetic frequency, ω_{Dj} is the magnetic drift frequency, ω is the frequency of the unstable mode, $\epsilon_{nj} = \omega_{Dj}/\omega_{\star j}$, $L_{nj} = -n_j/n_j'$ and $L_{Tj} = -T_j/T_j'$ are the density and temperature scale lengths for the particle species j and $\eta_j = L_{nj}/L_{Tj}$. From the density response, the particle fluxes can be calculated, $\Gamma_{nj} = \langle \delta n_j \boldsymbol{v}_j \rangle$. The impurity diffusion coefficient D_z, defined by $\Gamma_{nz} = -D_z \partial n_z/\partial r$ is then given by

$$D_z = 2\bar{\gamma}^3 \frac{\rho_s c_s}{R k_\theta} (\Delta_1 - \Delta_T \eta_z + 2\Delta_2 L_{nz}/R), \tag{8}$$

where γ and $\boldsymbol{k}$ are the linear growth rate and the wave number of the unstable mode, r and θ are radial and poloidal coordinates, $\rho_s = c_s/\Omega_{ci}$, $c_s = \sqrt{T_e/m_i}$ is the sound speed, $\Delta_T = 2\tau_z(\bar{\omega}_r + 5\tau_z/3)/|\bar{N}_z|^2$, the overbar denotes normalization with respect to the electron magnetic drift frequency ω_{De}, $\tau_z = T_z/(ZT_e)$,

$$\Delta_1 = [\bar{\omega}_r^2 + \bar{\gamma}^2 + 14\bar{\omega}_r\tau_z/3 + 55\tau_z^2/9]/|\bar{N}_z|^2,$$

$$\Delta_2 = -[\bar{\omega}_r^2 + \bar{\gamma}^2 + 10\bar{\omega}_r\tau_z/3 + 35\tau_z^2/9]/|\bar{N}_z|^2,$$

where $|\bar{N}_z|^2 = N_{zr}^2 + N_{zi}^2$, with $N_{zr} = \bar{\omega}_r^2 - \bar{\gamma}^2 + 10\tau_z\bar{\omega}_r/3 + 5\tau_z^2/3$ and $N_{zi} = 2\bar{\gamma}(\bar{\omega}_r + 5\tau_z/3)$. These expressions neglect impurity finite-Larmor-radius (FLR) effects and are in agreement with the corresponding ones given in Ref. 9. In Eqs. (7) and (8) the parallel dynamics of the impurities has been neglected based on the ordering $k_\| v_{Tz} < k_\| v_{Ti} < \omega$, which can be verified *a posteriori*. Here v_{Tj} is the thermal velocity of species j. In the quasilinear expressions, the space scale of the turbulence is fixed by choosing $(k_r\rho_s)^2 = (k_\theta\rho_s)^2 = 0.1$, corresponding to the scale of the fastest growing mode. To elucidate the physics for the magnetic shear dependence of impurity transport, we compare a strong ballooning analysis with bounce-averaged trapped electrons with the original formulation of the Weiland model[10] for deeply trapped electrons using a shear dependent eigenfunction.

1. Strong ballooning approximation

Using the semilocal analysis of Ref. 19, the eigenvalue equation is reduced to a set of 7 coupled algebraic equations for main and impurity ITG modes and collisionless TE modes. The ion/impurity and trapped electron fluid models are fairly symmetric, except that the electron FLR effects can be neglected. Here, the parallel dynamics of the impurities has been neglected. A strongly ballooning eigenfunction $[\phi = (1/\sqrt{3\pi})(1+\cos\theta), |\theta| < \pi]$ is used to calculate the norms of the operators $k_\|^2$, $k_\perp^2$, and $\omega_{Di,z}$ as

$$\langle k_\|^2 \rangle = 1/3(qR)^2, \tag{9}$$

$$\langle k_\perp^2 \rangle = k_\theta^2 [1 + (\pi^2/3 - 5/2)s^2], \tag{10}$$

$$\langle \omega_{Di,z} \rangle = \epsilon_{ni,z} \omega_{\star i,z} (2/3 + 5s/9), \tag{11}$$

where

$$\langle \cdots \rangle = \int_{-\pi}^{\pi} \phi(\cdots)\phi d\theta. \tag{12}$$

The strong ballooning approximation used here is only expected to give results in qualitative agreement with the full eigenvalue solution[19] and is not valid in the region close to $s=0$ where the width of the eigenfunction diverges. In the fluid treatment of the trapped electrons the electron magnetic drift is, after the bounce averaging, replaced by the precession frequency of trapped electrons as $\langle \omega_{De} \rangle = \omega_{De}\lambda_t$ where the parameter $\lambda_t = 1/4 + 2s/3$ characterizes the dependence of the precession frequency on the magnetic shear s.[22] The original formulation of the trapped electron treatment in the Weiland model for deeply trapped electrons is recovered for $\lambda_t = 1$ (see Sec. II A 2). A similar model, with $k_\perp^2$, $\omega_{Di,z}$ evaluated at $\theta = 0$ and neglecting the effects of impurities, was recently used to study parametric dependences of particle

transport[23] including qualitative comparisons with kinetic results.[24]

2. Shear dependent eigenfunction

In order to treat the transition from strong to weak ballooning in regions of weak magnetic shear, the analytical method of Ref. 18 is used to solve the eigenvalue equation for general mode width. The model is based on the same set of equations [Eqs. (1)–(3)] as used in the strong ballooning analysis but also includes the parallel dynamics of the impurities. In the analytical approach, the eigenfunction is assumed to be a Gaussian with

$$\phi \propto \exp(-\alpha\theta^2), \tag{13}$$

where θ is the extended poloidal angle and α is proportional to the magnitude of magnetic shear and the growth rate [see Eq. (3) of Ref. 18]. The sign is chosen so that the eigenfunction is localized for unstable modes. The coefficient α is determined by asymptotic matching for large θ. The norms of $\omega_{Di,z}$ and parallel wavenumber $k_\parallel$ are then evaluated as averages over the eigenfunction as in (12).

The derivation in Ref. 18 was made for the pure ITG mode but can be generalized as long as the asymptotic form of the eigenfunction does not change. The new physics then influences the eigenfunction only through the growth rate. Since the eigenfunction depends on the eigenfrequency ω, iteration is used to solve the resulting eigenvalue equation. Thus, an approximation for ω is chosen based on local theory and then the linear set of equations is solved. A new ω is obtained and the process is repeated until it converges. The eigenvalues are then used in the analytical expression for the effective impurity diffusivity D_z. Note that in this case, the original formulation of the Weiland model for deeply trapped electrons ($\lambda_t=1$) is used. The results are usually not sensitive to the choice of the trapped electron model due to the dominance of the ITG mode for the parameters considered in this paper.

3. Gyrokinetic calculations

The gyrokinetic results given in the present paper are based on flux-tube (local) simulations with the GYRO code.[28] Transport coefficients are computed including nonlinear gyrokinetic dynamics of both ion species. Since we are interested in ion-scale fluctuations only, at wavenumbers $k_\theta\rho_s<1.0$, the electron physics was taken to be the drift-kinetic, although the true electron mass was used $m_D/m_e=3600$. For the geometry model, we have used a circular Miller equilibrium[29] (i.e., although the flux-surface is an unshifted circle, it is an exact solution of the Grad-Shafranov equation). This will be useful for future work which moves away from circular plasmas to include the crucial effect of plasma shape (elongation, for example) on transport.

A 128-point velocity-space grid (8 energies, 8 pitch angles, and 2 signs of velocity) is used, together with 10 poloidal (orbit) grid points per sign of velocity. In the perpendicular directions (x,y), we content ourselves with a domain size of approximately $(L_x,L_y)/\rho_s=(122,128)$. Previous studies[8] have shown that this domain size gives an answer which is sufficiently close (within a few percent) to the infinite-box limit, whereas a $(L_x,L_y)/\rho_s=(64,64)$ box underestimates the transport level by roughly 25%. Here, x denotes the radial direction, and y denotes the binormal direction such that $L_y=2\pi/(k_\theta)_{\min}$. In the x direction we have $n_r=128$ radial grid points (so that $\Delta r/\rho_s=0.96$). In the y direction, we retain $n_n=16$ complex Fourier modes. With these choices, we resolve up to $(k_\theta)_{\max}\rho_s=0.74$. Simulations were run for a relatively long time; namely, $(c_s/a)t=1000$, and transport coefficients are derived from time averages over the interval $500\leqslant(c_s/a)t\leqslant1000$.

B. Neoclassical transport

Impurities in high-temperature plasmas, like ITER are expected to be in the banana regime. The neoclassical impurity flux in this regime is given by[25]

$$\langle \mathbf{\Gamma}_z\cdot\nabla\psi\rangle = \frac{f_t}{f_c}\frac{n_iT_iI^2\xi_z\left\{\tilde{\mu}_{z1}[\tilde{\mu}_{i1}(\ln p_i)' + \tilde{\mu}_{i2}(\ln T_i)'] - \dfrac{T_z\tilde{\mu}_{i1}}{T_iZ}[\tilde{\mu}_{z1}(\ln p_z)' + \tilde{\mu}_{z2}(\ln T_z)']\right\}}{m_iZ\Omega_{ci}^2\tau_{ii}(\tilde{\mu}_{i1}+\xi_z\tilde{\mu}_{z1})}, \tag{14}$$

where $\xi_z=\tau_{ii}m_zn_z(\tau_{zz}m_in_i)^{-1}$ and τ_{aa} is the collision time, f_t and f_c is the effective fraction of trapped and circulating particles, respectively. The magnetic field is $\boldsymbol{B}=I\nabla\varphi+\nabla\varphi\times\nabla\psi$, $\psi=-RA_\varphi$ is the poloidal flux-function, and the prime denotes derivative with respect to ψ. The normalized viscosity coefficients are $\tilde{\mu}_{ij}=m_j^{ii}+m_j^{iz}\alpha$ and $\tilde{\mu}_{zj}=(m_j^{zi}/\alpha\sqrt{Z})+m_j^{zz}$, with $\alpha=n_zZ^2/n_i$, and $m_1^{ab}=\sqrt{1+x_{ab}^2}+x_{ab}^2\ln[x_{ab}/(1+\sqrt{1+x_{ab}^2})]$, $m_2^{ab}=1/\sqrt{1+x_{ab}^2}-5m_1^{ab}/2$, where $x_{ab}=v_{Tb}/v_{Ta}$. The neoclassical flux depends on the safety factor q but is not sensitive to the derivative of q.

If Z is large, the neoclassical flux is mainly driven by ion gradients, since the coefficient multiplying the impurity gradients is Z times less than the coefficient multiplying the ion gradients. If the transport driven by impurity gradients can be neglected, the neoclassical flux is outward due to temperature screening if $\eta_i\gtrsim-\tilde{\mu}_{i1}/(\tilde{\mu}_{i1}+\tilde{\mu}_{i2})$ (assuming the density and temperature gradients have the same sign) and inward otherwise. For moderate or low Z, the flux driven by the impurity gradients will reduce the total impurity flux, since it has an opposite sign to the flux driven by the ion

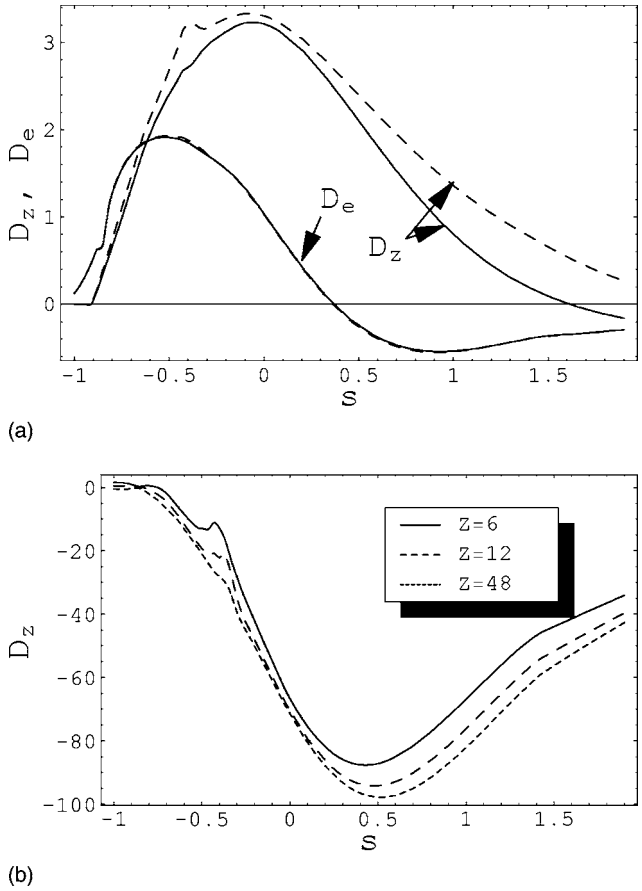

FIG. 1. (a) Shear scaling of effective diffusivities D_e and D_z in units of $2\rho_s^2 c_s/R$ using the strong ballooning approximation for $R/L_{Te}=R/L_{Ti}=9$, and $R/L_{Tz}=3$ (solid), $R/L_{Tz}=9$ (dashed). The other parameters are $Z=6$, $A_z=12$, $f_z=0.02$, $f_t=0.5$, $q=2$, $T_i=T_z=T_e$, and $R/L_{ne}=R/L_{nz}=3$. (b) Shear scaling of D_z for $R/L_{nz}=0.1$, $Z=6$ (solid), $Z=12$ (dashed), and $Z=48$ (dotted). The rest of the parameters are the same as in (a) with $R/L_{Tz}=9$.

gradients. In the following we denote the background and impurity ion gradient driven fluxes with D_z^i and D_z^z, respectively.

III. SHEAR DEPENDENCE

Due to the magnetic shear-dependence of the magnetic drifts and norms defined in Sec. II A, the eigenvalues of the unstable ITG and TE modes and the turbulent impurity transport depend on magnetic shear. In this section we will illustrate this by calculating the effective impurity diffusivity as a function of shear, keeping the temperature and density scale lengths of the different species as parameters. In the cases we present below, the neoclassical diffusivity is about an order of magnitude less than the turbulent diffusivity, and will not affect the main results.

In Fig. 1(a) the effective electron diffusivity D_e and impurity diffusivity D_z obtained using strong-ballooning approximation are displayed as a function of magnetic shear s, with R/L_{Tz} as a parameter. The results are shown for $R/L_{Ti}=R/L_{Te}=9$, i.e., far above marginal stability, with $R/L_{Tz}=3$ (solid) and $R/L_{Tz}=9$ (dashed). The other parameters are impurity charge $Z=6$, impurity mass $A_z=12$, fraction of impurities $f_z=0.02$, fraction of trapped electrons $f_t=0.5$, safety factor $q=2$, and $R/L_{ne}=R/L_{nz}=3$. For these parameters, the ITG mode is the dominant instability. The results show that the electron diffusivity can change sign as s is varied, as reported in Refs. 23 and 24. The strong shear scaling of the electron diffusivity is a result of the explicit dependence of D_e on the bounce averaged electron magnetic drift $\langle\omega_{De}\rangle \propto 1/4+2s/3$. The impurity diffusivity D_z is strongly reduced for negative and large positive shear through the ITG/TE eigenvalues. The results also show that the effect of a large impurity temperature gradient ($R/L_{Tz}=9$) in the present ITG dominated case is to increase the effective impurity diffusivity. This result is consistent with the results reported in Ref. 9 using the trace-impurity approximation which showed that the thermodiffusive contribution to the impurity flux is directed outwards for modes rotating in the ion direction when the parallel impurity velocity perturbation is neglected.

To investigate the magnetic shear scaling of the impurity pinch, Fig. 1(b) displays the effective impurity diffusivity versus shear using a flat impurity density profile, with $R/L_{nz}=0.1$. The other parameters are the same as in Fig. 1(a) with the impurity charge Z as a parameter varying from $Z=6$ (solid), to $Z=12$ (dashed) and $Z=48$ (dotted), while keeping $Zf_Z=0.12$ constant. As observed, the impurity pinch is directed inwards in this parameter regime. This is expected since the curvature pinch,[17] which is weakly dependent of Z, dominates in this regime. The slight increase of the impurity pinch with impurity charge Z is consistent with the reported Z scaling of the thermodiffusive contribution to the impurity flux ($\sim 1/Z$), which is outwards in this case.[9]

In Figs. 2(a) and 2(b) the corresponding results using the more general approach with a shear dependent eigenfunction are displayed. Due to the shear dependence of the width of the eigenfunction (13) the transport is strongly reduced for weak shear and increased for large positive shear as compared to the results of the strong ballooning analysis.

For the neoclassical transport calculations the following parameters were used in addition to the quantities given above: temperature $T_i=T_e=T_z=5$ keV, ion density $n_i=10^{20}$ m^{-3}, major radius $R=6.2$ m, and minor radius $a=2$ m. The neoclassical impurity transport is calculated using the large-aspect ratio, circular cross section approximation and it is in this case inward. The neoclassical diffusion coefficient which is independent of shear is $D_z^{\text{neo}}=-0.08$ for $R/L_{Tz}=3$ and $D_z^{\text{neo}}=-0.15$ for $R/L_{Tz}=9$ (in units of $2\rho_s^2 c_s/R$). This is smaller than the turbulent transport and would act to reduce the total impurity transport since it has the opposite sign as the turbulent flux (but will not affect the overall shape of the curve). However for sufficiently large negative shear the ITG/TE modes are stabilized and the neoclassical contribution dominates. The main reason that the neoclassical transport is so small in this case is the cancellation between the ion density gradient driven flux (inwards) and ion temperature gradient and impurity density gradient driven fluxes (outwards). For $R/L_{Tz}=3$ the ion gradient driven flux is $D_z^i=-0.29$ and the impurity gradient driven flux is $D_z^z=0.21$. For the case $R/L_{Tz}=9$, the impurity temperature gradient drives an additional inward flux and in this case $D_z^z=0.14$.

In Fig. 3 the effective electron and impurity diffusivities

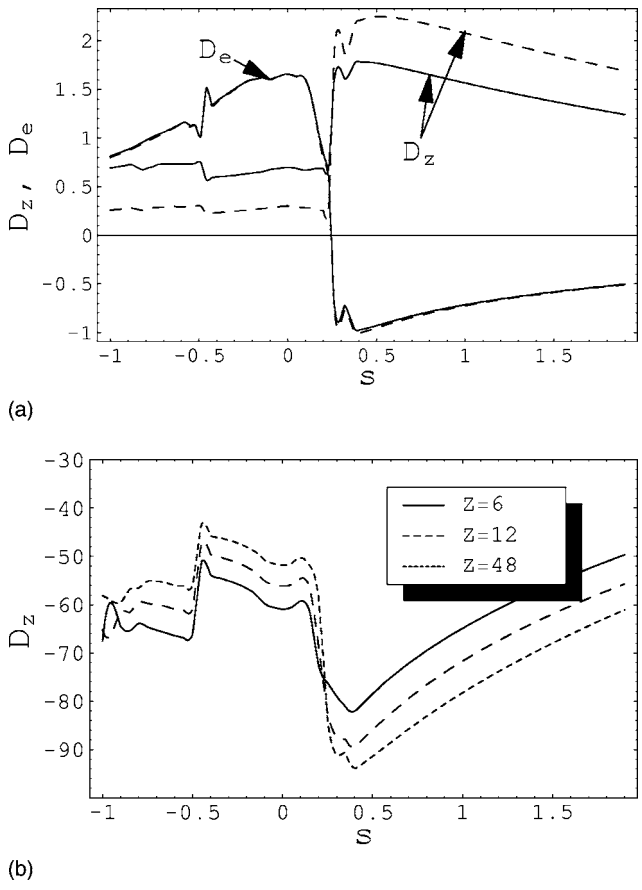

FIG. 2. Shear scaling of effective diffusivities in units of $2\rho_s^2 c_s/R$ for the same parameters as Figs. 1(a) and 1(b), using a shear-dependent eigenfunction.

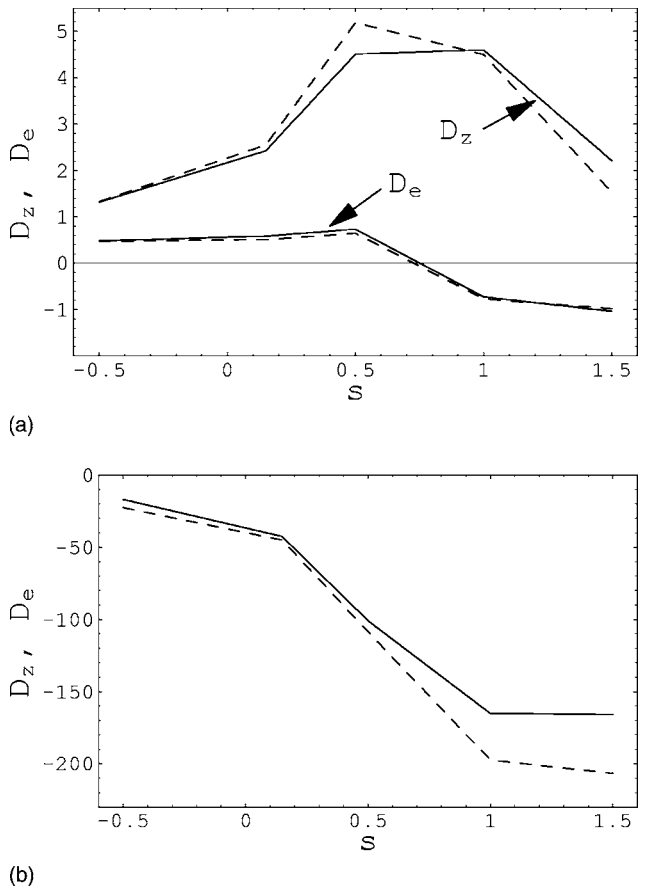

FIG. 3. (a) Shear scaling of effective diffusivities D_e and D_z in units of $2\rho_s^2 c_s/R$ for the same parameters as Fig. 1(a), using nonlinear gyrokinetic simulations. (b) Shear scaling of D_z for $R/L_{nz}=0.1$, $Z=6$ (solid), $Z=12$ (dashed). The rest of the parameters are the same as in Fig. 1(a) with $R/L_{Tz}=9$.

obtained using nonlinear gyrokinetic simulations are displayed for the same parameters as in Fig. 1. As observed, the fluid results of Figs. 1 and 2 of the shear scaling of the diffusivities are in qualitative agreement with the gyrokinetic results. The transport level, however, is typically a factor of 2 larger in the gyrokinetic case. Considering the differences between the fluid and kinetic models used in this study only qualitative agreement is expected.

In Fig. 4 the shear dependence of the effective impurity diffusivity is illustrated in regions closer to marginal stability (for smaller values of R/L_{Tj}) for $Z=6$, $A_z=12$, $f_z=0.02$, $f_t=0.5$, $R/L_{ne}=R/L_{nz}=2/3$, and $R/L_{Tj}=6$ (solid), $R/L_{Tj}=5$ (dashed) and $R/L_{Tj}=4$ (dotted). The results obtained for the strong ballooning eigenfunction [Fig. 4(a)] and the shear dependent eigenfunction [Fig. 4(b)] are in qualitative agreement.

For these density profiles parameters, the inward impurity pinch dominates the outward diffusive flux and the result is a negative effective impurity diffusivity. The neoclassical impurity transport is now outwards since the temperature screening is more effective in this case when the ion density gradient is flatter than it was in the case shown in Fig. 1. The neoclassical diffusion coefficients in these cases are $D_z^{\mathrm{neo}}=D_z^i+D_z^z=1.02-0.037=0.98$ for $R/L_{Tj}=6$, $D_z^{\mathrm{neo}}=D_z^i+D_z^z=0.73-0.011=0.72$ for $R/L_{Tj}=5$, $D_z^{\mathrm{neo}}=D_z^i+D_z^z=0.44+0.015=0.45$ for $R/L_{Tj}=4$. Also in these cases the neoclassical and turbulent transport have opposite signs, but the neoclassical is smaller.

In Fig. 5 the magnetic shear scaling of the ITG/TE mode eigenvalues is illustrated for the same parameters as in Fig. 1(a). The results of the strong ballooning analysis [Fig. 5(a)] are compared with the more general approach using a shear-dependent eigenfunction [Fig. 5(b)]. As observed, the ITG mode is usually the dominant instability for the considered parameters. We note that the assumption $k_\parallel v_{Tz} < k_\parallel v_{Ti} < \omega$ is satisfied for the ITG mode. The ITG growth rate is reduced for negative and large positive shear, in qualitative agreement with the gyrokinetic results and also with the gyrokinetic/gyrofluid results presented in Refs. 26 and 27. This is the main reason for the reduction of the impurity transport in these regions. The comparison confirms that the strong ballooning analysis grossly overestimates the ITG growth rate for weak shear where the assumption of a localized eigenfunction is not valid. Figures 5(a) and 5(b) also show that the TE mode eigenvalues depend sensitively on the treatment of the trapped electrons, in particular in regions of negative magnetic shear. In Fig. 5(a) the results of the bounce averaged TE model ($\lambda_t=1/4+2s/3$) shows a complete stabilization of the TE mode as the precession frequency $\langle \omega_{De} \rangle$ changes sign. In Fig. 5(b) on the other hand,

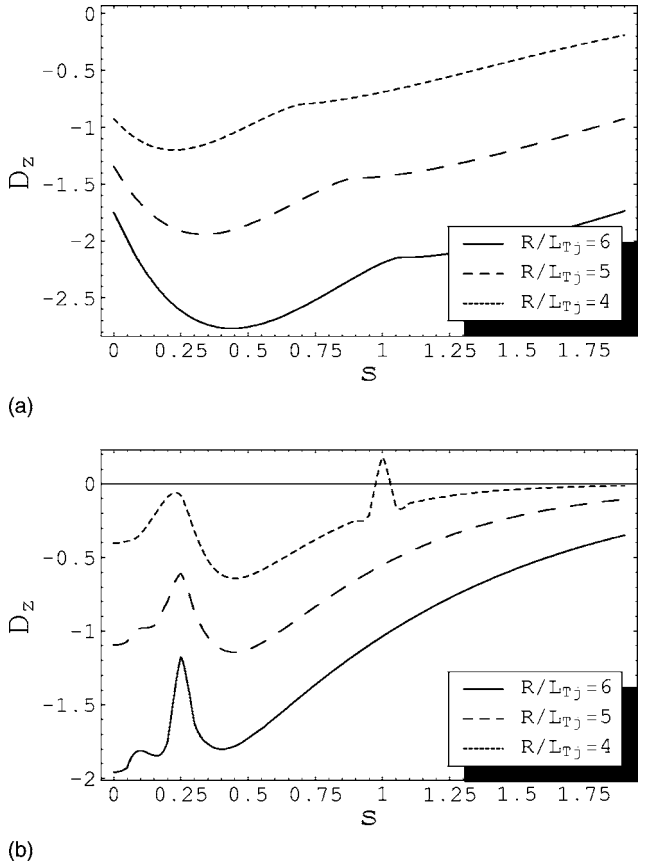

FIG. 4. (a) Effective impurity diffusivity D_z (in units of $2\rho_s^2 c_s/R$) versus magnetic shear for $R/L_{Tj}=6$ (solid), $R/L_{Tj}=5$ (dashed) and $R/L_{Tj}=4$ (dotted), $j=i$, z, e represent ions, impurities and electrons. The other parameters are $Z=6$, $A_z=12$, $f_z=0.02$, $f_t=0.5$, $q=1.4$, $T_i=T_z=T_e$, and $R/L_{ne}=R/L_{nz}=2/3$. (b) Same as (a) but with shear-dependent eigenfunction.

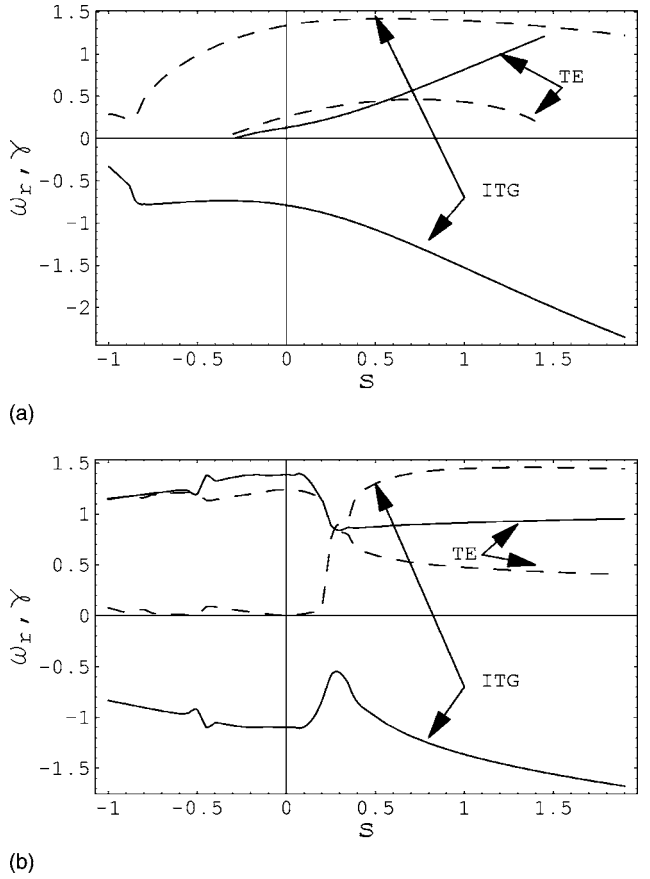

FIG. 5. Real part of the frequency ω_r (solid) and the growth rate γ (dashed) of the unstable ITG and TE modes (normalized to ω_{*e}) using the strong ballooning approximation as functions of magnetic shear corresponding to case (a) with $R/L_{Tz}=9$ in Fig. 1. (b) Same as (a) but with shear-dependent eigenfunction.

the corresponding results of the TE model for deeply trapped electrons ($\lambda_t=1$) gives a strong TE mode in this region.

Steady-state values of density gradients can be calculated from the condition of zero particle fluxes in source-free plasmas. For given plasma parameters with $Z=6$, $f_z=0.033$, $q=1.4$, and $R/L_T=9$, a double scan in R/L_{ne} and R/L_{nz} is performed and the curves of zero electron and impurity flux and their intersection is identified. In this calculation, the neoclassical part of the flux has been neglected. The results using the shear dependent eigenfunction are displayed in Fig. 6 for $s=0.8$ (solid) and for $s=0.2$ (dashed). For $s=0.8$ we obtain $R/L_{ne}=4.7$ and $R/L_{nz}=1.5$ in steady state. The corresponding results for $s=0.2$ are $R/L_{ne}=0.8$ and $R/L_{nz}=2.7$. We have verified that these results scale rather weakly with other plasma parameters, for example the impurity charge Z and the fraction of impurities f_z. The results show that the predicted steady-state impurity profile is generally less peaked than the electron density profile for moderate and large shear. For weak shear, however, the opposite result is obtained.

IV. ITER

In order to illustrate the shear dependence of the anomalous impurity flux for ITER-like parameters and compare it to neoclassical fluxes, an ITER scenario[20] is studied. The selected scenario is a hybrid-mode, with a plasma current of 12 MA, major radius $R=6.2$ m, minor radius $a=2$ m, and magnetic field $B=5.3$ T. Figure 7 displays the safety-factor, magnetic shear and normalized temperature gradient param-

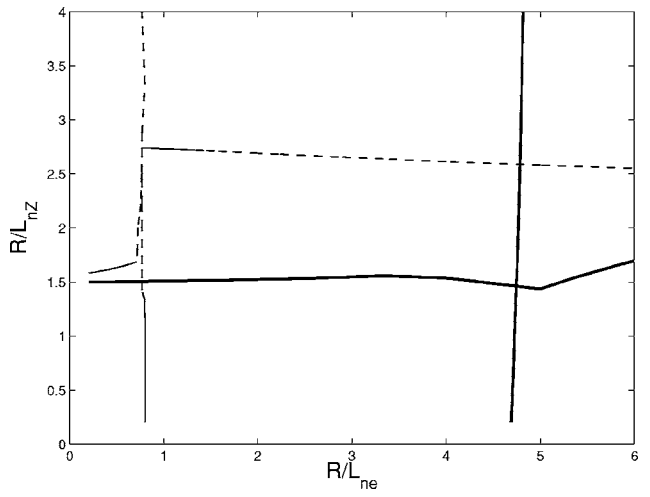

FIG. 6. Contour plots showing particle fluxes $\Gamma_{ne}=0$ and $\Gamma_{nz}=0$ versus R/L_{ne} and R/L_{nz} for magnetic shear $s=0.8$ (solid) and $s=0.2$ (dashed). The other parameters are $Z=6$, $A_z=12$, $f_z=0.033$, $q=1.4$, $T_i=T_z=T_e$, and $R/L_{Tj}=9$. The results are obtained using the shear dependent eigenfunction.

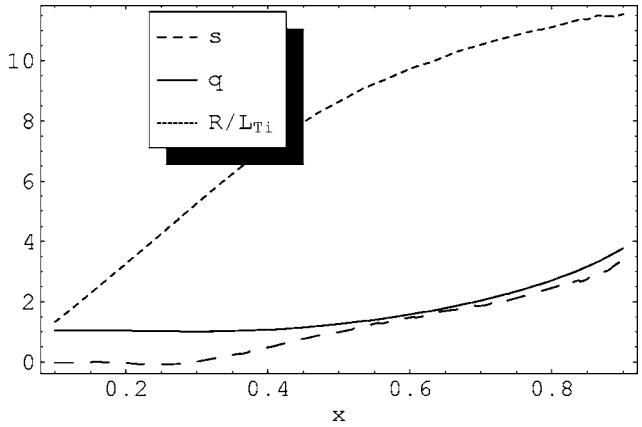

FIG. 7. Safety factor (solid), shear (dashed), and R/L_{Ti} (dotted) for the selected ITER-like scenario as a function of normalized radius.

eter R/L_{Ti} and Fig. 8 shows the ion and impurity density and ion and electron temperature profiles for this ITER scenario. The impurity and ion temperatures are assumed to be equal.

The turbulent impurity flux is calculated using the two analytical models (presented in Secs. II A 1 and II A 2) for $Z=6$ (including impurity FLR-effects for completeness) and the results are compared with a local version of the model (with $\lambda_t=1$, and $k_\perp^2$, $\omega_{Di,z}$ evaluated at $\theta=0$) which is independent of magnetic shear. Figure 9 shows the impurity fluxes and Fig. 10 shows the corresponding real frequencies

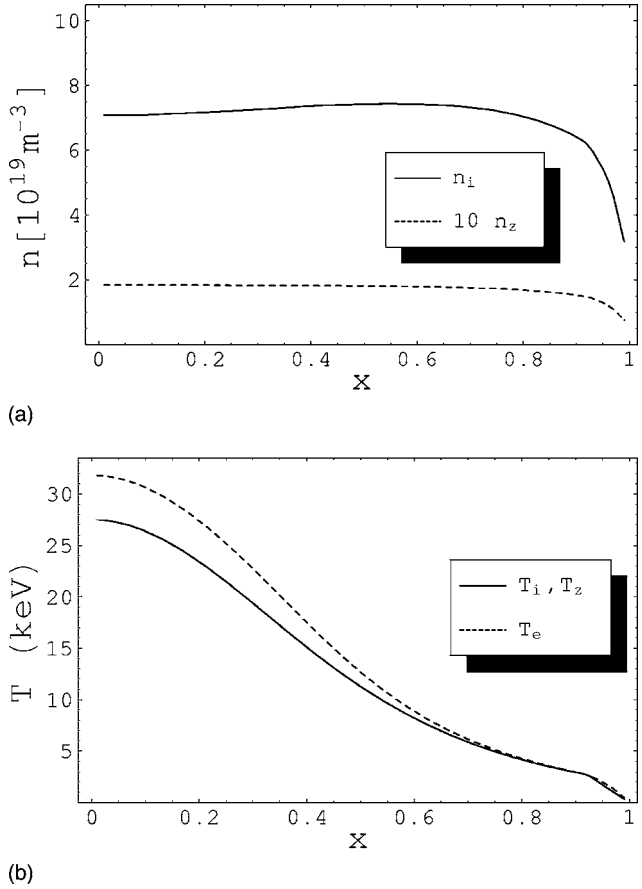

FIG. 8. Radial density and temperature profiles as a function of normalized minor radius for the selected ITER-like scenario.

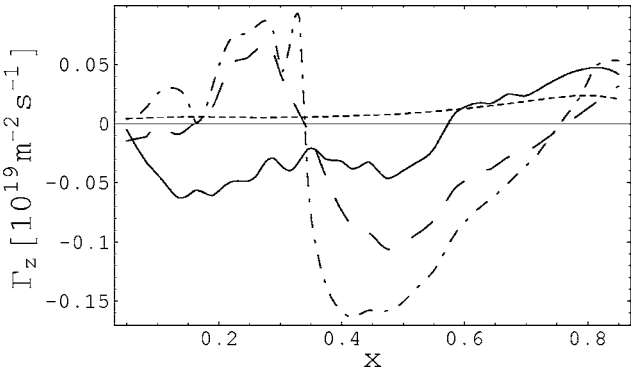

FIG. 9. Turbulent and neoclassical impurity fluxes for an ITER-like scenario and $Z=6$ as a function of normalized radius. The solid line corresponds to a fluid model without magnetic shear dependence, the dashed is the fluid model using the strong ballooning approximation, the dashed-dotted is the fluid model using the shear dependent eigenfunction. The dotted line corresponds to the neoclassical impurity flux.

and growth rates of the unstable modes. We note that the results of the shear dependent models differ significantly from the results of the local analysis. The reason for the sudden change in the impurity flux around $r/a \simeq 0.35$ is that the magnetic shear of the selected ITER scenario varies from $s=0$ at $r/a=0.3$ to $s=0.5$ at $r/a=0.4$. This change in the shear affects the impurity transport strongly, so that it even reverses its sign. The reason for the large inward pinch at $r/a=0.4$ is that the magnetic shear is close to $s \simeq 0.5$ where the impurity pinch is strongest [see Figs. 1(b) and 2(b)]. As a result of this, the turbulent flux is inwards in the central part of the plasma but outwards in the inner core $r/a \lesssim 0.3$ and outside $r/a \gtrsim 0.7$. The neoclassical transport is mainly driven by the background ion gradients and is outwards due to temperature screening.

Interestingly, for this ITER-like case, turbulent and neoclassical transport are of the same order of magnitude. In this ITER scenario the density profile is very flat and therefore the neoclassical transport is mainly driven by the temperature gradient. In the previous section, the assumed R/L_{nj} was much larger, and since the density gradient driven transport

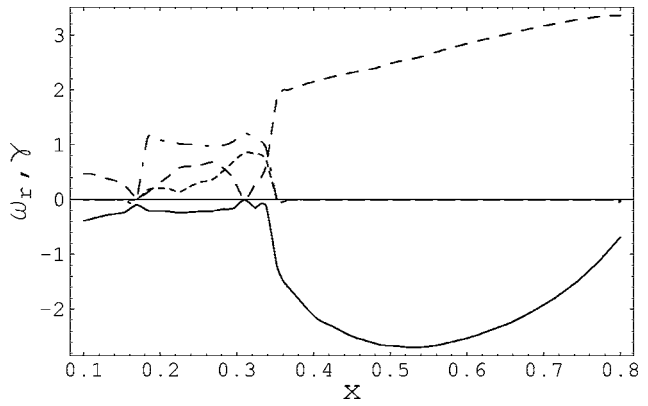

FIG. 10. Real part of the frequency ω_r and growth rate γ of the unstable ITG and TE modes (normalized to ω_{*e}), for the selected ITER-like scenario as functions of normalized radius, using the fluid model with the shear-dependent eigenfunction. The solid and dashed-dotted lines are ω_r and the dashed and dotted lines are γ for the ITG and TE-modes, respectively.

has an opposite sign to the temperature gradient driven transport, this resulted in a much smaller neoclassical than turbulent transport in those cases.

V. CONCLUSIONS

We have studied the magnetic shear scaling of impurity transport using a fluid model of ITG/TE mode driven turbulence, nonlinear gyrokinetic simulations, and neoclassical theory. In general, the shear dependence of the impurity diffusivity is found to be weaker than that of the electron diffusivity. However, for weak, negative, and large positive shear, a strong reduction of the effective impurity diffusivity is obtained. The fluid and gyrokinetic models give qualitatively similar results for the shear scaling of the impurity transport. However the fluid diffusivities are typically a factor 2 lower than the corresponding gyrokinetic diffusivities. Close to the TE mode stability threshold, corresponding to the inner core region of tokamak plasmas, a reduction of the effective impurity diffusivity is obtained due to the stabilization of the TE mode with magnetic shear. For typical parameters values, the reduction occurs for $0.5<s<1$. The results obtained using the strong ballooning analysis are in qualitative agreement with the results of the more general approach valid for general mode width except in the region close to $s=0$ where the strong ballooning approximation breaks down.

The steady state density scale lengths in source free plasmas, i.e., for zero particle flux, have been calculated. The results indicate that ITG/TE mode turbulence supports a more peaked electron density profile than impurity density profile for moderate shear. The impurity peaking is found to depend of magnetic shear, with more peaked profiles obtained for weak shear. The impurity peaking is consistent with the results reported in Ref. 7.

We have compared the anomalous and neoclassical impurity transport for a hybrid ITER scenario. The results show that for the selected ITER-like collisionless plasma with flat density profile, turbulent and neoclassical transport have opposite signs in the central part of the plasma. In the inner core $r/a<0.3$ and outside $r/a>0.7$ both neoclassical and turbulent transport are outwards.

ACKNOWLEDGMENT

This work was funded by the European Communities under Association Contract between EURATOM and *Vetenskapsrådet* and U.S. Department of Energy Grant DE-FG03-95ER54309.

[1] P. H. Rebut, Nucl. Fusion **25**, 1011 (1985).
[2] Tore Supra Team, Nucl. Fusion **40**, 1047 (2000).
[3] R. Gianella, L. Lauro-Taroni, M. Mattioli, B. Alper, B. Denne-Hinnov, G. Magyar, J. O'Rourke, and D. Pasini, Nucl. Fusion **34**, 1185 (1994).
[4] M. Mattioli, C. De Michelis, and A. L. Pecqouet, Nucl. Fusion **38**, 1629 (1998).
[5] S. Günter, C. Angioni, M. Apostoliceanu, C. Atanasiu *et al.*, Nucl. Fusion **45**, S98 (2005).
[6] R. Dux, A. G. Peeters, A. Gude, A. Kallenbach, R. Neu, and ASDEX Upgrade Team, Nucl. Fusion **39**, 1509 (1999).
[7] R. V. Budny, C. E. Kessel, J. E. Kinsey, F. Imbeaux *et al.*, "Transport Physics of Hybrid Scenario Plasmas in the International Multi-Tokamak Database and Implications for ITER," IAEA conference Chengdu (2006).
[8] C. Estrada-Mila, J. Candy, and R. E. Waltz, Phys. Plasmas **12**, 022305 (2005).
[9] C. Angioni and A. G. Peeters, Phys. Rev. Lett. **96**, 095003-1 (2006).
[10] J. Weiland, *Collective Modes in Inhomogeneous Plasma* (IOP Bristol, 2000).
[11] M. Fröjdh, M. Liljeström, and H. Nordman, Nucl. Fusion **32**, 419 (1992).
[12] J. Q. Dong, S. M. Mahajan, and W. Horton, Phys. Plasmas **4**, 755 (1997).
[13] R. Paccagnella, F. Romanelli, and S. Briguglio, Nucl. Fusion **30**, 545 (1990).
[14] S. P. Hirshman and D. J. Sigmar, Nucl. Fusion **21**, 1079 (1981).
[15] P. I. Strand, G. Bateman, A. Eriksson, W. A. Houlberg *et al.*, Proceedings of the 31st EPS Conference on Plasma Physics, 2004, London, Vol. 28 G, p. 5.187.
[16] T. Fülöp and J. Weiland, Phys. Plasmas **13**, 112504 (2006).
[17] X. Garbet, L. Garzotti, P. Mantica, H. Nordman, M. Valovic, H. Weisen, and C. Angioni, Phys. Rev. Lett. **91**, 035001-1 (2003).
[18] J. Weiland, Phys. Plasmas **11**, 3238 (2004).
[19] A. Hirose, Phys. Fluids B **5**, 230 (1993).
[20] A. Polevoi (private communication, 2006).
[21] M. R. Wade, W. A. Houlberg, L. R. Baylor, W. P. West, and D. R. Baker, J. Nucl. Mater. **290–293**, 773 (2001).
[22] X. Garbet, N. Dubuit, E. Asp, Y. Sarazin, C. Bourdelle, P. Ghendrih, and G. T. Hoang, Phys. Plasmas **12**, 082511 (2005).
[23] H. Nordman, P. Strand, and X. Garbet, Proceedings of the 33rd EPS Conference on Plasma Physics, 2006, Rome, Vol. 30 I, p. 4.163.
[24] J. E. Kinsey, R. E. Waltz, and J. Candy, Phys. Plasmas **13**, 022305 (2006).
[25] P. Helander and D. J. Sigmar, *Collisional Transport in Magnetized Plasmas* (Cambridge University Press, Cambridge, 2002).
[26] R. E. Waltz, G. M. Staebler, W. Dorland, G. W. Hammett, M. Kotschenreuther, and J. A. Konings, Phys. Plasmas **4**, 2482 (1997).
[27] G. M. Staebler, J. E. Kinsey, and R. E. Waltz, Phys. Plasmas **12**, 102508 (2005).
[28] J. Candy and R. E. Waltz, J. Comput. Phys. **186**, 545 (2003).
[29] R. L. Miller, M. S. Chu, J. M. Greene, Y. R. Lin-liu, and R. E. Waltz, Phys. Plasmas **5**, 973 (1998).